Editors' Suggestion

Uncertainty growth in stably stratified turbulence

Mrinal Jyoti Powdel [*] and Samriddhi Sankar Ray [†]
International Centre for Theoretical Sciences,
Tata Institute of Fundamental Research, Bengaluru 560089, India

(Received 2 January 2026; accepted 8 May 2026; published 23 June 2026)

We investigate uncertainty growth and chaotic dynamics in statistically steady, stably stratified three-dimensional turbulence. Using direct numerical simulations of the Boussinesq equations, we quantify the divergence of initially infinitesimal perturbations via twin simulations and decorrelator diagnostics. At short times, perturbations exhibit exponential growth, allowing us to define a (largest) Lyapunov exponent. We systematically examine how this exponent depends on stratification strength, quantified by the Brunt-Väisälä frequency and the Froude number, in a parameter regime relevant to oceanic flows. We find that increasing stratification leads to a monotonic reduction of the Lyapunov exponent, indicating suppressed chaoticity. Despite this reduction, uncertainty growth retains the universal temporal sequence observed in homogeneous isotropic turbulence—initial decay, exponential growth, and saturation. The growth phase is characterized by self-similar decorrelator spectra, but exhibits strong anisotropy: uncertainty spreads much more slowly along the stratification direction than horizontally, with the disparity increasing with stratification strength. An analysis of the decorrelator evolution equation reveals that the suppression of chaos arises primarily from strain-mediated alignment dynamics rather than direct buoyancy coupling. Our results provide a quantitative characterization of predictability and uncertainty growth in stratified turbulence and highlight the utility of decorrelator-based methods for anisotropic geophysical flows.

DOI: 10.1103/xblr-vpl3

I. INTRODUCTION

Predictability in turbulent flows is a central problem in fluid mechanics, with direct relevance to weather forecasting, climate modeling, oceanic transport, and environmental dispersion. Even for the idealized case of homogeneous and isotropic turbulence, the quantitative characterization of sensitivity to infinitesimal perturbations remains incomplete. Classical arguments due to Ruelle [1] linked the largest Lyapunov exponent λ to Kolmogorov phenomenology, predicting a scaling with the smallest dynamically active time scale τ_η. Subsequent developments incorporating intermittency corrections and multifractal models [2,3] refined these ideas [4]. Advances in direct numerical simulations (DNSs) over the past two decades have enabled increasingly precise measurements of Lyapunov exponents in homogeneous and isotropic turbulence, yet discrepancies between theoretical predictions, model systems, and numerical data persist, underlining the subtle nature of chaos in turbulent flows [5–8].

One such approach that has proved useful to probing sensitivity in high-dimensional dynamical systems is to track the time evolution of the difference between two initially nearly identical states evolved under the same dynamics. We call the key quantity of interest in this approach as the

[*]Contact author: mrinal.jyoti@icts.res.in
[†]Contact author: samriddhisankarray@gmail.com

 ©2026 American Physical Society

decorrelator [9], which quantifies how velocity or scalar fields diverge in time and space. Applications of such methods in dynamical systems and turbulence, dating from the seminal works of Lorenz [10] and Leith and Kraichnan [11], has been widely used to study the growth of predictibility or uncertainty in homogeneous isotropic turbulent flows [12–17], in elastic turbulence [18], and in quasigeostrophic turbulence [19]. Such diagnostics provide a direct, nonperturbative measure of uncertainty growth and allow one to extract Lyapunov exponents as well as study the spatial structure and scale-by-scale propagation of perturbations. Recent applications of this framework to fully developed turbulence [16,20] and similar nonlinear hydrodynamic equations [21,22] have revealed a robust dynamical sequence: an initial decay of perturbations followed by a period of exponential growth with a self-similar spectrum and eventual saturation. Remarkably, this appears to be universal for three-dimensional turbulence [20].

While homogeneous and isotropic, fully developed turbulence provides a fundamental reference state, most natural flows of geophysical relevance differ markedly from this idealization. The oceans and atmosphere are often strongly influenced by stable density stratification, which introduces buoyancy forces, supports internal gravity waves through the Brunt-Väisälä frequency N, and imposes a preferred vertical direction [23–27]. Stratified turbulence is therefore intrinsically anisotropic and arises from the nonlinear interaction of vortical motions and wave dynamics. Decades of theoretical, numerical, and experimental work have established that stratification suppresses vertical motions at low Froude numbers, promotes the formation of layered structures, and alters energy transfer pathways relative to homogeneous and isotropic turbulence [28–46]. While these effects are now well understood at the level of flow structure and energetics, their consequences for the chaotic dynamics of turbulence—including the rate of uncertainty growth, the spreading of perturbations in space, and the overall predictability of stratified flows—have received comparatively little attention.

Predictability and sensitivity to initial conditions in stratified flows have been explored in several settings, but predominantly for decaying or rotational turbulence. In such studies [47], predictability is typically characterized using relative error growth or predictability times in decaying and not statistically stationary dynamics. Lagrangian approaches [48–50] based on finite-time Lyapunov exponents and particle separation have been widely applied to study Lagrangian coherent structures in oceanic flows. However, the influence of stable stratification on Eulerian chaos and predictability in statistically stationary turbulence remains largely unresolved.

In this work, we address this gap by studying uncertainty growth in forced, statistically stationary three-dimensional stably stratified turbulence governed by the Boussinesq equations. Using pseudospectral direct numerical simulations, we perform twin simulations that differ by an infinitesimal, localized perturbation at the initial time and track the evolution of velocity and buoyancy differences across time and scales. This Eulerian decorrelator framework enables the direct extraction of the largest Lyapunov exponent λ and a detailed characterization of anisotropic uncertainty spectra as a function of stratification strength. We show that increasing stratification systematically suppresses chaoticity, primarily through a reduction of nonlinear strain and enhanced strain-buoyancy alignment, rather than through direct buoyancy effects. These results establish a quantitative link between stratification, anisotropy, and chaotic dynamics over a range of Brunt-Väisälä frequencies relevant to oceanic conditions.

II. GOVERNING EQUATIONS, NUMERICAL METHODS, AND PARAMETERS

Density-stratified turbulent flows require lifting the constant-density approximation commonly employed for homogeneous and isotropic incompressible turbulence. A stratification is stable when the fluid density $\rho(\mathbf{x})$ satisfies $d\rho(\mathbf{x})/dz < 0$. For stable stratification, the simplest background state consists of a constant vertical density gradient $-\gamma$ imposed on a reference density ρ_0 at $z = z_0$. In turbulent geophysical flows, however, density fluctuations induced by motion must also be accounted for, so that the total density field reads

$$\rho(\mathbf{x}, t) = \rho_0 - \gamma(z - z_0) + \rho_f(\mathbf{x}, t),$$

where ρ_f denotes the fluctuating component and gravity acts as $\mathbf{g} = -g\hat{\mathbf{z}}$. In the ideal, inviscid, and unforced limit, such a background stratification supports small-amplitude vertical oscillations of fluid parcels [23] with characteristic Brunt-Väisälä frequency $N = \sqrt{g\gamma/\rho_0}$.

In the atmosphere, density variations with height are typically large, whereas in oceanic flows they are comparatively small [51]. These differences motivate distinct reduced descriptions of stratified geophysical flows: the anelastic approximation is commonly used for atmospheric dynamics, while the Boussinesq approximation is appropriate for weakly stratified fluids such as the ocean. In this work, we employ the Boussinesq formulation.

The Boussinesq approximation is valid when the total density variations—arising from both the background stratification $\Delta\rho(z) = -\gamma(z - z_0)$ and the fluctuating component $\rho_f(\mathbf{x}, t)$—are small compared with the reference density ρ_0. Under this condition, density variations can be neglected everywhere except in the buoyancy term, where they provide the restoring force associated with stable stratification.

It is convenient to work with the buoyancy field $b = (\rho_f N)/\gamma$, which has the same physical dimensions as the velocity field. The governing equations for stably stratified turbulence are then

$$\frac{\partial \mathbf{u}}{\partial t} + \mathbf{u}\cdot\boldsymbol{\nabla}\mathbf{u} = \nu\nabla^2\mathbf{u} - \boldsymbol{\nabla}p + Nb\,\hat{\mathbf{z}} + \mathbf{f}, \tag{1}$$

$$\frac{\partial b}{\partial t} + \mathbf{u}\cdot\boldsymbol{\nabla}b = \kappa\nabla^2 b - N\,\mathbf{u}\cdot\hat{\mathbf{z}}, \tag{2}$$

supplemented by the incompressibility condition $\boldsymbol{\nabla}\cdot\mathbf{u} = 0$. The external forcing $\mathbf{f}$ injects energy and maintains a statistically steady turbulent state. In the inviscid and unforced limit, the Boussinesq system conserves the total energy, given by the sum of kinetic and potential energy, even though these components can exchange through buoyancy coupling.

We solve these equations using pseudospectral direct numerical simulations (DNSs) in a triply periodic domain of size 2π, with up to 512^3 collocation points and a second-order Runge–Kutta time-marching scheme. The kinematic viscosity is fixed at $\nu = 5\times10^{-3}$, yielding Taylor-scale Reynolds numbers $100 \lesssim \mathrm{Re}_\lambda = u_{\mathrm{rms}}^2\sqrt{15/(\epsilon\nu)} \lesssim 130$, where u_{rms} is the root-mean-square velocity and ϵ is the mean kinetic energy dissipation rate (the precise value depending on N). We set the Prandtl number $\mathrm{Pr} = \nu/\kappa$ to unity, appropriate for thermally stratified flows, though not representative of salt-stratified systems where Pr may be much larger. Simulations are performed for $N = 0$ (the unstratified reference case) and for $N = 1, 4, 7$, and 12.

In this paper, we refer $\perp$ as the direction perpendicular to the axis (here, z axis) of stratification. The flow is driven by a constant power injection applied only to the horizontal velocity components (i.e., perpendicular direction). The forcing is vortical [46,52–54] and restricted to modes with $k_z = 0$. In Fourier space, it is given by

$$\tilde{\boldsymbol{f}}_\perp(\mathbf{k}_\perp, k_z, t) = \begin{cases} \frac{1}{M}\frac{\mathcal{P}}{2E_K^{(m)}}\,\tilde{\mathbf{u}}_\perp(\mathbf{k}_\perp, k_z, t), & (|\mathbf{k}_\perp|, k_z) = (m, 0), \\ 0, & \text{otherwise}, \end{cases} \tag{3}$$

with $\tilde{f}_z = 0$. Here M is the number of forced modes, $E_K^{(m)}$ is the horizontal kinetic energy in the $(m, 0)$ mode, and $\mathcal{P}$ is the prescribed power input. In all runs, we force modes with $m = 1, 2$, so that $M = 2$.

Although N^{-1} defines the characteristic time scale associated with stratification—analogous to the Kolmogorov time scale $\tau_\eta = \sqrt{\nu/\epsilon}$—its dynamical influence is more conveniently quantified by the Froude number $\mathrm{Fr} = u_{\mathrm{rms}}/(\ell N)$, where ℓ is the integral length scale obtained from the kinetic energy spectrum $E_K(k)$. In our simulations, $0.09 \lesssim \mathrm{Fr} \lesssim 0.97$, such that $\mathrm{Fr} < 1$ and the buoyancy Reynolds number $\mathrm{Re}_b \sim \mathrm{Re}_\lambda \mathrm{Fr}^2$ exceeds unity. Together with $\mathrm{Re}_\lambda \gg 1$, these conditions place our flows in the strongly stratified turbulence regime.

To assess geophysical relevance, we compare our parameters with typical oceanic values. Observations [55–57] indicate $O(10^{-3}\,\mathrm{s}^{-1}) \lesssim N \lesssim O(10^{-1}\,\mathrm{s}^{-1})$. Using representative oceanic values $\nu = 10^{-6}\,\mathrm{m}^2/\mathrm{s}$ [58] and $\epsilon = 10^{-6}\,\mathrm{m}^2/\mathrm{s}^3$ [59] yields $\tau_\eta \simeq 1\,\mathrm{s}$ and hence a dimensionless Brunt-

Väisälä frequency $\tilde{N} = N\tau_\eta$ in the range $O(10^{-3}) \lesssim \tilde{N} \lesssim O(10^{-1})$. This overlaps with the values explored here, $0.082 \lesssim \tilde{N} \lesssim 1$ (with $N = \tilde{N} = 0$ corresponding to the unstratified reference state).

Similarly, observed oceanic values of root-mean-square velocities ($0.1\,\mathrm{m/s} \lesssim u_{\mathrm{rms}} \lesssim 2\,\mathrm{m/s}$) and integral length scales [$O(10^4)\,\mathrm{m} \lesssim \ell \lesssim O(10^5)\,\mathrm{m}$] [60] imply Froude numbers in the range $O(10^{-4}) \lesssim \mathrm{Fr} \lesssim O(10^{-2})$, consistent with the regime probed by our simulations, albeit at lower Reynolds numbers than those of the ocean.

III. UNCERTAINTY GROWTH AND LYAPUNOV EXPONENTS

To quantify the sensitivity of stratified turbulence to infinitesimal perturbations and thereby characterise uncertainty growth, we employ a twin-flow construction in which two nearly identical states are evolved under identical dynamics.

We begin by constructing statistically steady stratified turbulent states for different values of the nondimensional Brunt-Väisälä frequency $\tilde{N} = N\tau_\eta$. Let $\mathbf{u}_0^{\mathrm{A}}$ and b_0^{A} denote the velocity and buoyancy fields of such a nonequilibrium steady state. A second, nearly identical flow B is then initialised according to

$$\mathbf{u}_0^{\mathrm{B}} = \mathbf{u}_0^{\mathrm{A}} + \epsilon_0 \boldsymbol{\nabla} \times \mathbf{A}, \quad b_0^{\mathrm{B}} = b_0^{\mathrm{A}},$$

where $\epsilon_0 \ll 1$.

The perturbation $\epsilon_0 \boldsymbol{\nabla} \times \mathbf{A}$ is chosen to be small, localized, symmetric, and divergence free. Explicitly, the vector potential, $\mathbf{A}$ has components

$$A_i = \sqrt{\frac{3u_{\mathrm{rms}}^2}{2}}\, r_0 \exp\left[-\frac{(\mathbf{x} - \mathbf{x}_0)^2}{2r_0^2}\right]\hat{e}_i,$$

with localization scale $r_0 \ll 2\pi$ and center at $\mathbf{x}_0 = (\pi, \pi, \pi)$. This choice ensures that the perturbation is confined to a small region of the domain while preserving incompressibility.

Systems A and B are then evolved independently under identical dynamics. At any later time t, this allows us to define the velocity and buoyancy difference fields

$$\delta\mathbf{u}(\mathbf{r}, t) \equiv \mathbf{u}^{\mathrm{B}} - \mathbf{u}^{\mathrm{A}}, \quad \delta b(\mathbf{r}, t) \equiv b^{\mathrm{B}} - b^{\mathrm{A}}.$$

By construction, $\delta\mathbf{u}(\mathbf{r}, 0) = \epsilon_0 \boldsymbol{\nabla} \times \mathbf{A}$ and $\delta b(\mathbf{r}, 0) = 0$. The perturbation is introduced only to the velocity field while the buoyancy field is left undisturbed. The choice of not perturbing the buoyancy field is motivated by the observation that the velocity field is the primary dynamical variable, while buoyancy acts as an active scalar coupled to the flow. However, the coupled nature of both the fields ensure that at $t = 0^+$, the difference in the buoyancy field is rendered a nonzero value, after which both $\delta\mathbf{u}$ and δb evolve dynamically.

Figure 1 shows representative pseudocolor plots of the velocity decorrelator $\phi^u(\mathbf{x}, t) = \frac{1}{2}|\delta\mathbf{u}(\mathbf{x}, t)|^2$ for a typical stratified run, with $\tilde{N} = 0.99$, at an early time $t/\tau_\eta = 84.10$ during the decorrelation process. We display two-dimensional slices taken in the [Fig. 1(a)] XY and [Fig. 1(b)] XZ planes. The insets correspond to an earlier instant $t/\tau_\eta = 24.03$, before exponential growth sets in. These visualizations reveal the emergence of strongly anisotropic structures, which proliferate in time and elongate horizontally while remaining compressed in the vertical direction. In particular, our results indicate an inhibited spread of uncertainty in z due to buoyancy effects.

To quantify uncertainty growth, we consider the spatially averaged decorrelator

$$\Phi^u(t) = \langle \phi^u(\mathbf{x}, t) \rangle,$$

where angular brackets denote a volume average. Figure 2(a) shows the temporal evolution of $\Phi^u(t)$ for several values of the nondimensional Brunt-Väisälä frequency, $\tilde{N}$. For all cases, $\Phi^u(t)$ displays a common sequence of dynamical regimes. At very early times, $\Phi^u(t)$ exhibits a slight decay [bottom inset of Fig. 2(a)], reflecting the rapid viscous relaxation of the imposed perturbation. We do not have a precise quantitative understanding of the dependence of this decay on, for example,

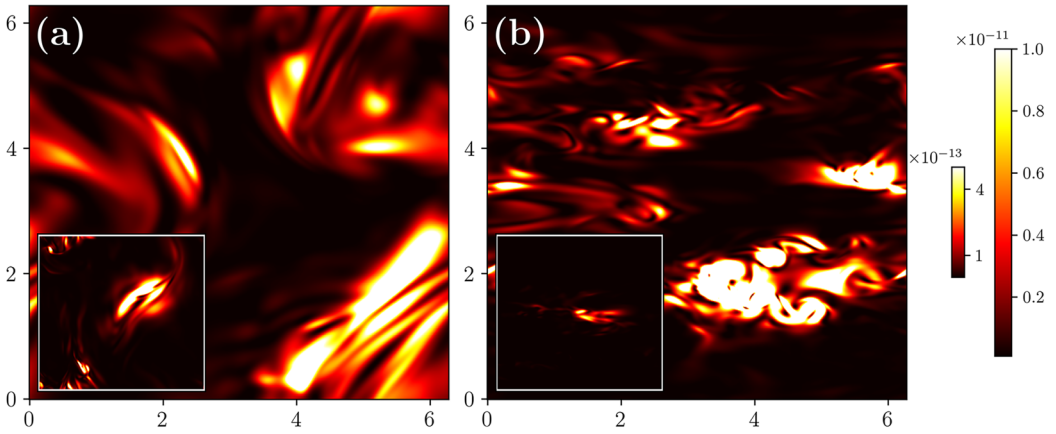

FIG. 1. Pseudocolor plots of $\phi_u(\mathbf{x}, t) = \frac{1}{2}|\delta\mathbf{u}(\mathbf{x}, t)|^2$ for a representative stratified run with $N = 12$ ($\tilde{N} = 0.99$) during the early stages of decorrelation for slices in the (a) XY and (b) XZ planes. Insets correspond to an earlier time before exponential growth begins. The inner color bar corresponds to the inset, while the outer colorbar corresponds to the main figure. The perturbation field develops pronounced anisotropy, forming extended structures perpendicular to the direction of stratification. The reduced vertical variability highlights the suppression of uncertainty propagation along the stratification axis due to buoyancy effects.

the Froude number; indeed our analysis from several numerical realizations suggests that this transient decay phase is perhaps nonuniversal and sensitive to the exact flow configuration (even in statistical steady state) when the perturbation is introduced. This initial decay phase is followed by a pronounced, universal growth phase in which $\Phi^u(t)$ increases exponentially in time before eventually saturating, as zoomed in in the top inset, once the two flow realizations become fully decorrelated.

We make a comment on the timescales at which the decorrelator saturates. For thermalized, Hamiltonian fluids where the velocity fields are Gaussian and the spectrum equipartitions [61], it is shown [21] that the saturation timescale is proportional to the decay time scale of its autocorrelation function, and the inverse of the Lyapunov exponent, with proportionality constants of $O(1)$. We have checked for a similar relation in stratified turbulence and found numerically that in this case the proportionality constant is $O(10)$.

The existence of a clear exponential growth regime allows us to define a Lyapunov exponent λ characterizing the rate of uncertainty amplification. Extracting λ from the slope of $\ln \Phi^u(t)$ during this interval, we find that the degree of chaoticity decreases systematically as stratification strengthens. As shown in Fig. 2(b), the normalized Lyapunov exponent $\lambda\tau_\eta$ decreases monotonically with increasing $\tilde{N}$, indicating that stable stratification suppresses sensitivity to infinitesimal perturbations. The same trend is evident in Fig. 2(b) when λ is plotted against the Froude number, confirming that enhanced buoyancy effects lead to a dynamically calmer regime compared to homogeneous and isotropic turbulence at comparable Reynolds numbers.

We have also computed the corresponding buoyancy decorrelator, $\Phi_b(t) = \langle \frac{1}{2}|\delta b(\mathbf{x}, t)|^2 \rangle$, and verified that it exhibits the same exponential growth rate as $\Phi_u(t)$ during the chaotic regime (not shown). This reflects the coupling between velocity and buoyancy perturbations in Eqs. (1)–(2), which causes both fields to be slaved to the same dominant strain dynamics. In a similar spirit, one might be motivated to explore other measures of uncertainty growth, possibly involving both the velocity and the buoyancy field. The simple most natural example of such a quantity is the cross correlator $\langle \delta u_z \delta b \rangle$. This cross correlator appears explicitly in the decorrelator evolution equation, Eq. (4) and is analyzed in Fig. 3(a). As can be seen, it remains subdominant [compared to $\Phi^u(t)$] throughout the evolution and even becomes negative as the two systems A and B decorrelate,

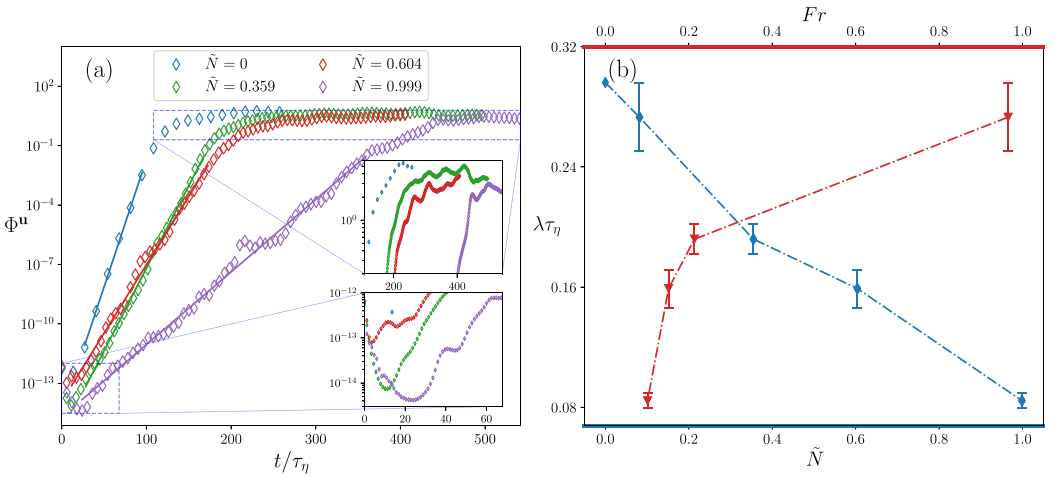

FIG. 2. (a) A semilog plot of the temporal evolution of the spatially averaged velocity decorrelator $\Phi^u(t) = \langle \frac{1}{2}|\delta\mathbf{u}(\mathbf{x}, t)|^2\rangle$ for different values of the nondimensional Brunt-Väisälä frequency $\tilde{N}$ (see legend) is shown along with two insets zooming in on different stages of the evolution. After an initial decay (bottom inset), $\Phi^u(t)$ exhibits a clear exponential growth regime followed by saturation (top inset), indicating complete decorrelation of the two flow realizations. The open diamonds are the values obtained from DNS and the solid lines indicate fits using the values of $\lambda\tau_\eta$. (b) The Lyapunov exponent λ in units of Kolmogorov time scale τ_η extracted from the exponential growth phase of $\Phi^u(t)$ as a function of $\tilde{N}$ (lower axis). The monotonic decrease of λ with increasing stratification strength shows that stable stratification systematically suppresses chaoticity. The same data is also plotted against the Froude number Fr (upper axis), confirming that increased buoyancy effects lead to reduced sensitivity to infinitesimal perturbations.

consistent with total energy conservation of the coupled velocity-buoyancy system. Other cross correlators like $\langle \delta u_x \delta b\rangle$ and $\langle \delta u_y \delta b\rangle$ were not considered, as they did not appear in a natural way from the governing equations.

Before we turn to an understanding of the exponential growth of the decorrelators in the next section, we end with a remark on the scale dependence of the Froude number and how it determines the turbulence of stratified flows. The Froude number, by definition, is scale dependent. In particular, at the Kolmogorov scale $\mathrm{Fr}_\eta = \tilde{N}^{-1} = (N\tau_\eta)^{-1}$. For the flow to be stratified at every scale $\mathrm{Fr}_\eta \lesssim 1$. This is the regime where $\tilde{N} > 1$. In this regime, Eqs. (1) and (2) can be approximated by their linear counterparts as shown in Ref. [62] with a vanishing Lyapunov exponent. Indeed, we do see in Fig. 2(b) a sharply decreasing $\lambda\tau_\eta$ with increasing $\tilde{N}$; however, given that we work in the stratified nonlinear turbulent regime, the question of how fast $\lambda\tau_\eta \to 0$ when $\tilde{N}$ becomes larger than unity is beyond the scope of this work.

IV. PHYSICAL INTERPRETATION OF UNCERTAINTY GROWTH

How can these observations be understood directly from the equations of motion? Following the framework developed in Refs. [16,20], we derive an evolution equation for the spatially averaged velocity decorrelator $\Phi^u(t)$:

$$\partial_t \Phi^u(t) = \beta_S + \beta_\eta + N\langle \delta u_z\, \delta b\rangle + \langle \delta\mathbf{f} \cdot \delta\mathbf{u}\rangle, \tag{4}$$

where $\beta_S = -\langle \delta\mathbf{u} \cdot \mathbf{S} \cdot \delta\mathbf{u}\rangle$ represents stretching and compression by the symmetric rate-of-strain tensor $\mathbf{S}$, and $\beta_\eta = \nu\langle \delta\mathbf{u} \cdot \nabla^2 \delta\mathbf{u}\rangle$ denotes viscous dissipation. In addition to the terms familiar from homogeneous and isotropic turbulence (HIT), stratification introduces the buoyancy-velocity cross correlation $N\langle \delta u_z\, \delta b\rangle$.

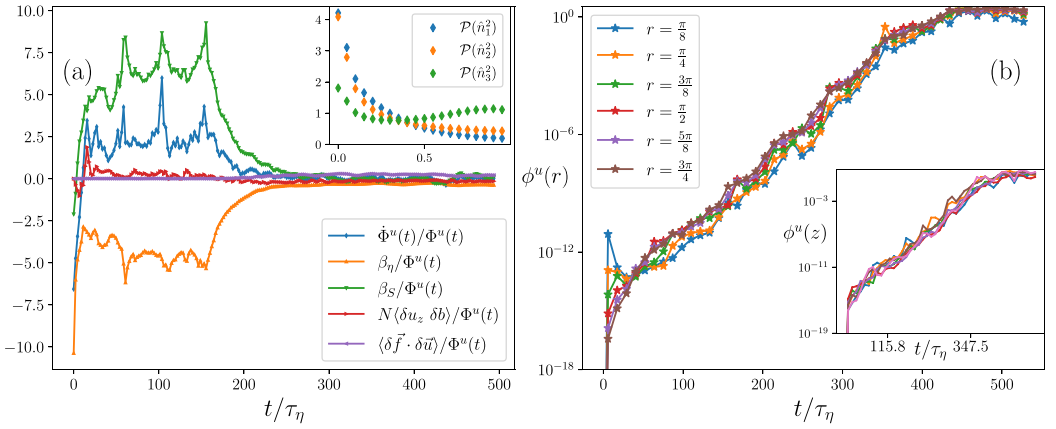

FIG. 3. (a) Time evolution of the individual contributions to the decorrelator growth rate in Eq. (4) for $\tilde{N} = 0.359$: the strain-induced term β_S, the viscous term β_η, the buoyancy-velocity cross correlation $N\langle\delta u_z\ \delta b\rangle$, and the forcing contribution, each normalized by $\Phi^u(t)$. The initial decay of $\Phi^u(t)$ is driven by large, negative contributions from β_S and β_η, while the buoyancy term remains subdominant throughout. The inset shows a comparison of the probability distributions of $\hat{n}_i^2$ during the early stages of the exponential growth phase (at $t/\tau_\eta = 6.76$) for $\tilde{N} = 0.359$ (b) Temporal evolution of the spherically averaged decorrelator $\phi^u(r,t)$ with respect to the center at $\mathbf{x}_0$ for different radii r (see legend) for the case of $\tilde{N} = 0.604$, illustrating spatially homogeneous exponential growth of uncertainty. The inset shows $\phi^u(z,t)$ at fixed r for seven different values of z in the range $0.53\pi \leqslant z \leqslant 1.47\pi$, confirming uniform growth even along the direction of stratification. The dashed curve represents the spectra for the reference state.

Direct evaluation of these contributions shows that, throughout most of the evolution and across all Froude numbers considered, the buoyancy-induced term remains subdominant compared to β_S and β_η, as illustrated in Fig. 3(a). Immediately after the perturbation is introduced, both $\beta_S/\Phi^u(t)$ and $\beta_\eta/\Phi^u(t)$ are large and negative, resulting in the initial decay of $\Phi^u(t)$ observed in Fig. 2(a). This transient reflects the rapid viscous relaxation of a perturbation that has not yet developed preferential alignment with local flow structures. The sharp spikes visible in Fig. 3(a) reflect the intrinsic intermittency of the velocity-gradient field and the instantaneous alignment statistics entering β_S, rather than discrete or dynamically distinct flow events.

Further insight is obtained by decomposing β_S in the eigenbasis of the rate-of-strain tensor,

$$\beta_S = -\sum_{i=1}^{3} n_i^2\,\gamma_i\,|\delta\mathbf{u}|^2,$$

where γ_i are the eigenvalues of $\mathbf{S}$ and n_i are the direction cosines of $\delta\mathbf{u}$ along the corresponding eigendirections. Such a decomposition, and the analysis of uncertainty growth in terms of the eigenstructure of the strain tensor and the role of compressive and extensional eigendirections, have been developed in previous works [16,18,20], where the importance of alignment between perturbations and strain eigendirections—and the resulting importance of compressive contributions in certain regimes—was highlighted. The largest eigenvalue $\gamma_1 > 0$ corresponds to the extensional direction, $\gamma_3 < 0$ to the compressional direction, while $\gamma_2 \approx 0$ is associated with a nearly neutral direction. At early times, the perturbation samples these eigendirections almost isotropically, so that $\sum_i n_i^2\gamma_i$ is negative on average and β_S contributes to decay. During the exponential growth phase, however, the perturbation aligns strongly with the compressional eigendirection ($n_3^2 \simeq 1$), while the contribution from extensional stretching gets suppressed. This preferential sampling of the compressional eigendirections are seen in the probability distribution functions of the three eigendirections as shown in the inset of Fig. 3(a). Thus, in this regime, $\beta_S + \beta_\eta$ becomes positive,

driving exponential uncertainty growth, while both the buoyancy-velocity correlator and forcing term remain negligible. This behavior is consistent with earlier studies [16,18,20], where the role of alignment with strain eigendirections in governing uncertainty growth was also emphasized. In particular, these works showed that the contribution of the strain term can be strongly influenced by preferential sampling of specific eigendirections. In the present case, however, stable stratification modifies these alignment dynamics through anisotropy and buoyancy effects. We find that increasing stratification enhances preferential alignment with the compressive eigendirection, which contributes to the observed suppression of the Lyapunov exponent.

A further hallmark of incompressible Navier-Stokes dynamics is the nonlocality of the pressure field, which implies that an imposed perturbation can influence distant regions of the flow essentially instantaneously. As a result, the growth of uncertainty is spatially homogeneous. This behavior is demonstrated in Fig. 3(b), where we show the temporal evolution of the spherically averaged decorrelator $\phi^u(r,t) = \langle \phi^u(\mathbf{x},t)\rangle$ for several values of the radius, $r = |\mathbf{x} - \mathbf{x}_0|$ with respect to the center, $\mathbf{x}_0$ of the initial perturbation. All radial shells exhibit identical exponential growth rates. One may go further and define $\phi^u(z,t)$ as the azimuthally averaged decorrelator with respect to the z axis passing through $\mathbf{x}_0$. The inset of Fig. 3(b) shows the evolution of $\phi^u(z,t)$ for various values of z in the shell defined by $r = \pi/2$. This further confirms this homogeneity by demonstrating that uncertainty growth remains uniform also along z direction despite the underlying anisotropy of stratified turbulence.

V. SPECTRAL AND ANISOTROPIC STRUCTURE OF UNCERTAINTY

The anisotropic nature of uncertainty growth, evident in the real-space decorrelator fields shown in Fig. 1, can be quantified more systematically in spectral space. Unlike homogeneous isotropic turbulence, stably stratified flows possess an inherent direction set by gravity, and the spread of uncertainty along the vertical (z) direction differs markedly from that in the horizontal plane. This motivates a scale-dependent analysis of the decorrelator using uncertainty spectra.

We define the velocity decorrelator spectrum as

$$\tilde{\phi}^u(\mathbf{k},t) = \tfrac{1}{2}\langle |\delta\tilde{\mathbf{u}}(\mathbf{k},t)|^2\rangle, \tag{5}$$

where $\delta\tilde{\mathbf{u}}(\mathbf{k},t)$ denotes the three-dimensional Fourier transform of $\delta\mathbf{u}(\mathbf{x},t)$, and $\langle\cdots\rangle$ represents an average over the spherical shell $|\mathbf{k}| = \text{const}$. This yields the isotropic uncertainty spectrum. To probe anisotropy, we additionally consider reduced spectra, $\tilde{\phi}^u(k_\perp,t)$ and $\tilde{\phi}^u(k_z,t)$, obtained by summing over wave vectors with fixed $k_\perp = \sqrt{k_x^2 + k_y^2}$ and fixed k_z, respectively.

Figure 4(a)–4(c) shows the temporal evolution of $\tilde{\phi}^u(k_\perp,t)$ for $\tilde{N} = 0.359$ across distinct phases of decorrelation. During the initial decay phase, uncertainty rapidly populates higher horizontal wave numbers. This is followed by a clear exponential-growth regime in which the spectrum evolves self-similarly. In this regime, the decorrelator spectrum exhibits the scaling form

$$\tilde{\phi}^u(k_\perp,t) \sim \ell_\perp^\Delta(t)\,\Phi^u(t)\,f(k_\perp \ell_\perp^\Delta(t)), \tag{6}$$

where f is a universal scaling function and $\ell_\perp^\Delta(t)$ is the uncertainty integral length scale in the perpendicular direction. It is important to state here explicitly that the universal scaling function f is also a function of the Froude number.

The integral scale is defined as

$$\ell_\perp^\Delta(t) = \frac{1}{\sum_{k_\perp}\tilde{\phi}^u(k_\perp,t)}\sum_{k_\perp}\frac{\tilde{\phi}^u(k_\perp,t)}{k_\perp}, \tag{7}$$

and measures the dominant horizontal scale over which uncertainty is distributed. The inset of Fig. 4(b) demonstrates this self-similarity for $\tilde{N} = 0.359$: when the spectra are rescaled by $\ell_\perp^\Delta(t)$ and $\Phi^u(t)$, they collapse onto a single curve during the exponential growth phase.

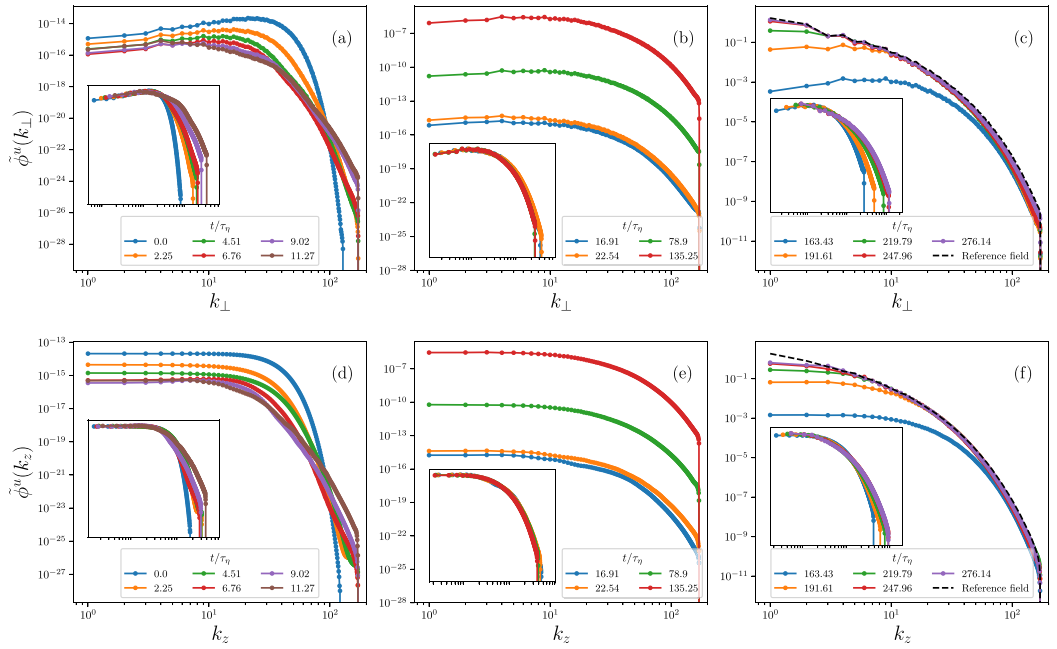

FIG. 4. Evolution of the uncertainty spectrum in spectral space for $\tilde{N} = 0.359$: (a)–(c) Horizontal decorrelator spectra $\tilde{\phi}^u(k_\perp, t)$ at representative times during the decay, exponential growth, and saturation phases. The inset shows the rescaled spectra $\tilde{\phi}^u(k_\perp, t)/[\ell_\perp^\Delta(t)\Phi^u(t)]$ plotted against $k_\perp \ell_\perp^\Delta(t)$. As can be seen from inset of (b), the rescaled spectra collapses demonstrating self-similar evolution in the growth phase. (d)–(f) The corresponding vertical decorrelator spectra $\tilde{\phi}^u(k_z, t)$, exhibiting analogous behavior along the direction of stratification.

It is important to emphasise that these uncertainty integral scales are global, energy-weighted measures constructed from the full decorrelator spectrum. As such, they are dominated by contributions from the largest dynamically active scales and do not necessarily reflect the strong local or morphological anisotropy visible in real-space decorrelator fields (Fig. 1). Pronounced horizontal elongation or vertical confinement at intermediate and small scales may therefore not translate into a large numerical separation between ℓ_z^Δ and $\ell_\perp^\Delta$.

As the decorrelator approaches saturation, uncertainty progressively invades lower wave numbers, indicating a transfer from small to large scales. Eventually, once the two realizations are completely decorrelated, the uncertainty spectrum converges to the kinetic energy spectrum of the reference flow,

$$\tilde{\phi}^u(k_\perp, t) \longrightarrow 2E_K(k_\perp), \tag{8}$$

shown by dashed black curves in Fig. 4(c). An analogous sequence of spectral phases is observed for the vertical spectrum $\tilde{\phi}^u(k_z, t)$, shown in Fig. 4(d)–4(f), as well as for the isotropic uncertainty spectrum (not shown). Similar self-similar evolution of decorrelator spectra was previously reported for homogeneous isotropic turbulence [16].

Strong stratification is known to suppress vertical velocity fluctuations, leading to flow structures with much smaller vertical length scales than horizontal ones. This anisotropy is reflected directly in the uncertainty dynamics for higher degree of stratification. As seen in Fig. 1, the decorrelator structures in the growth phase are elongated in the horizontal plane and compressed along z. This is because the buoyancy effects has a dominant effect in most of the length scales (even the smallest ones) in highly stratified flows. This behavior can be gauged from Fig. 5 for $\tilde{N} = 0.999$,

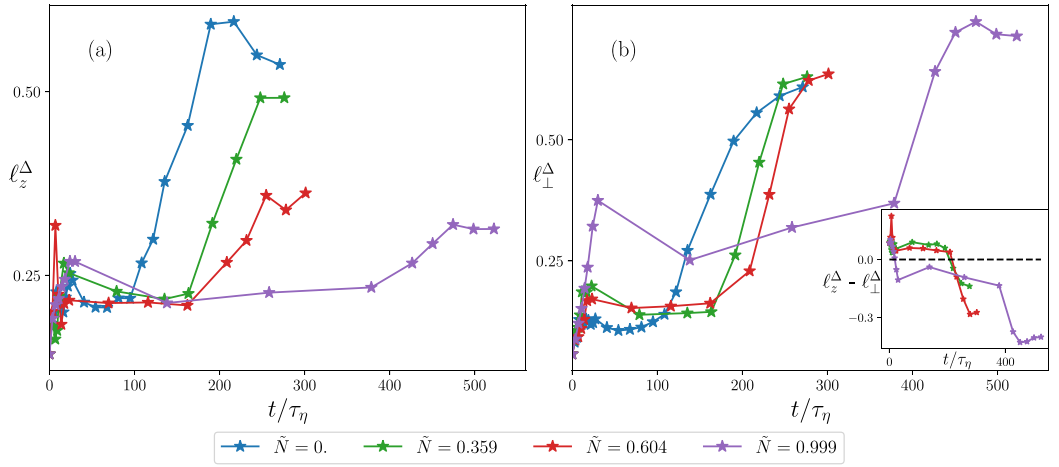

FIG. 5. Temporal evolution, across the transient decay, growth and saturation phase, of the uncertainty integral length scales in the (a) vertical (ℓ_z^Δ) and (b) horizontal ($\ell_\perp^\Delta$) directions for different $\tilde{N}$ suggesting an increased vertical confinement and an unrestricted horizontal spreading with increasing stratification. The inset in (b) shows the difference $\ell_z^\Delta - \ell_\perp^\Delta$ over the same time window.

by comparing the temporal evolution of the uncertainty integral length scales in the vertical (ℓ_z^Δ) and horizontal ($\ell_\perp^\Delta$) and directions. Through the exponential and the saturation phase, ℓ_z^Δ remains smaller than $\ell_\perp^\Delta$ for $\tilde{N} = 0.999$. However, for intermediate stratification strengths $\tilde{N} = 0.359$ and 0.604, this anisotropy is reflected only in the saturation phase of the decorrelator.

This behavior is best illustrated in a plot of the difference between the two length scales $\ell_z^\Delta - \ell_\perp^\Delta$ over time as shown in the inset of Fig. 5(b). Our choice of initial perturbation constrains $\ell_z^\Delta > \ell_\perp^\Delta$ at $t = 0$. For moderate stratification ($\tilde{N} = 0.359, 0.604$), this inequality persists throughout the exponential growth phase and reverses only when the decorrelator saturates. However, for our highest stratification ($\tilde{N} = 0.999$), the sign reverses already in the transient decay phase and persists all the way to the saturation regime. This behavior is consistent with our understanding of the increasingly dominant effect of buoyancy, across all scales, in highly stratified flows.

VI. CONCLUSIONS

We have investigated the growth of uncertainty in stably stratified turbulence using decorrelator-based diagnostics and Lyapunov analysis. Increasing stratification strength (decreasing Froude number) leads to a systematic reduction of the Lyapunov exponent, demonstrating that stable stratification suppresses chaoticity. Despite this quantitative change, uncertainty growth retains the familiar temporal structure observed in homogeneous isotropic turbulence: an initial decay phase, followed by self-similar exponential growth and eventual saturation.

The exponential growth regime is characterized by a universal, self-similar evolution of the uncertainty spectra. However, in contrast to isotropic flows, uncertainty propagation is anisotropic, especially, for highly stratified flows. Perturbation spread show more vertical confinement while being progressively unrestrained in the horizontal direction with increasing stratification.

Analysis of the decorrelator evolution equation reveals the physical origin of this reduced chaoticity. Stratification primarily acts by altering the alignment between perturbations and the local rate-of-strain tensor. During the exponential growth phase, perturbations preferentially align with compressive eigendirections, which is a feature one also finds in the case of isotropic turbulence. In contrast, buoyancy-velocity cross correlations, and forcing contributions remain subdominant, indicating that the suppression of chaos is controlled predominantly by strain-mediated dynamics rather

than direct buoyancy coupling. Although the Reynolds numbers achieved in our simulations remain lower than those characteristic of oceanic flows, similar limitations are common in direct numerical studies of stratified turbulence. Nevertheless, the systematic trends reported here—particularly the monotonic suppression of the Lyapunov exponent with increasing stratification and the anisotropic structure of uncertainty growth—are expected to persist at higher Reynolds numbers.

From a geophysical perspective, these findings suggest that strong stable stratification can enhance short-time predictability by limiting the vertical spread of uncertainty, even while permitting rapid horizontal error growth. Taken together, our results provide a quantitative characterization of uncertainty growth and Lyapunov dynamics in stratified turbulence. Beyond their implications for predictability in geophysical flows, this work establishes decorrelator-based methods as a robust framework for diagnosing chaotic dynamics in anisotropic and wave-supporting turbulent systems, with natural extensions to rotating, magnetized, and convectively driven flows. Furthermore, our observation that perturbations in the buoyancy and velocity fields grow with the same Lyapunov exponent raises the broader question of how universal this behavior is in turbulent systems with coupled fields. A similar phenomenon has been reported in magnetohydrodynamic turbulence [63]. However, a systematic investigation of this issue remains an interesting direction for future work. It would also be worthwhile to explore the relative advantages of decorrelator-based diagnostics compared with approaches based on finite-time Lyapunov exponents, as used, for example, in Ref. [8] for generic turbulent flows.

ACKNOWLEDGMENTS

M.J.P. and S.S.R. acknowledge several discussions with Arun Kumar Varanasi. M.J.P. also thanks Rajarshi and Sanjay C P for useful suggestions. S.S.R. acknowledges the Indo-French Centre for the Promotion of Advanced Scientific Research (IFCPAR/CEFIPRA, Project No. 6704-1) for support. The simulations were performed on the ICTS clusters Mario, Tetris, Boson2, and Contra. M.J.P. and S.S.R. acknowledge the support of the DAE, Government of India, under Projects No. RTI4013 and No. RTI4019.

DATA AVAILABILITY

There are no publicly available research data or software supporting this paper. Requests for further information or data should be sent to the authors.

[1] D. Ruelle, Microscopic fluctuations and turbulence, Phys. Lett. A **72**, 81 (1979).
[2] U. Frisch and G. Parisi, Turbulence and predictability of geophysical fluid dynamics and climate dynamics, in *Proceedings of the International School of Physics Enrico Fermi, Course LXXXVIII, Varenna* (North-Holland, Amsterdam, 1985).
[3] U. Frisch, *Turbulence: The legacy of A. N. Kolmogorov* (Cambridge University Press, Cambridge, 1995).
[4] A. Crisanti, M. H. Jensen, A. Vulpiani, and G. Paladin, Intermittency and predictability in turbulence, Phys. Rev. Lett. **70**, 166 (1993).
[5] J. Bec, L. Biferale, G. Boffetta, M. Cencini, S. Musacchio, and F. Toschi, Lyapunov exponents of heavy particles in turbulence, Phys. Fluids **18**, 091702 (2006).
[6] M. Cencini, F. Cecconi, and A. Vulpiani, *Chaos* (World Scientific, Singapore, 2009).
[7] S. S. Ray, Non-intermittent turbulence: Lagrangian chaos and irreversibility, Phys. Rev. Fluids **3**, 072601(R) (2018).
[8] R. D. J. G. Ho, D. Clark, and A. Berera, Chaotic measures as an alternative to spectral measures for analysing turbulent flow, Atmosphere **15**, 1053 (2024).

[9] A. Das, S. Chakrabarty, A. Dhar, A. Kundu, D. A. Huse, R. Moessner, S. S. Ray, and S. Bhattacharjee, Light-cone spreading of perturbations and the butterfly effect in a classical spin chain, Phys. Rev. Lett. **121**, 024101 (2018).
[10] E. N. Lorenz, The predictability of a flow which possesses many scales of motion, Tellus **21**, 289 (1969).
[11] C. E. Leith and R. H. Kraichnan, Predictability of turbulent flows, J. Atmos. Sci. **29**, 1041 (1972).
[12] P. Mohan, N. Fitzsimmons, and R. D. Moser, Scaling of Lyapunov exponents in homogeneous isotropic turbulence, Phys. Rev. Fluids **2**, 114606 (2017).
[13] S. Mukherjee, J. Schalkwijk, and H. J. J. Jonker, Predictability of dry convective boundary layers: An LES study, J. Atmos. Sci. **73**, 2715 (2016).
[14] G. Boffetta and S. Musacchio, Chaos and predictability of homogeneous-isotropic turbulence, Phys. Rev. Lett. **119**, 054102 (2017).
[15] A. Berera and R. D. J. G. Ho, Chaotic properties of a turbulent isotropic fluid, Phys. Rev. Lett. **120**, 024101 (2018).
[16] J. Ge, J. Rolland, and J. C. Vassilicos, The production of uncertainty in three-dimensional Navier–Stokes turbulence, J. Fluid Mech. **977**, A17 (2023).
[17] J. Ge, J. Rolland, and J. C. Vassilicos, The interscale behaviour of uncertainty in three-dimensional Navier–Stokes turbulence, J. Fluid Mech. **1017**, A29 (2025).
[18] J. R. C. King, R. J. Poole, C. P. Fonte, and S. J. Lind, Uncertainty in elastic turbulence, J. Fluid Mech. **1020**, A2 (2025).
[19] V. de Jesus Valadão, F. De Lillo, S. Musacchio, and G. Boffetta, Scaling and predictability in surface quasi-geostrophic turbulence, J. Fluid Mech. **1017**, A38 (2025).
[20] A. Banerjee, R. Mukherjee, S. D. Murugan, S. Bhattacharjee, and S. S. Ray, Intermittent fluctuations determine the nature of chaos in turbulence, Phys. Rev. Lett. (2026), doi:10.1103/1dj2-zw28.
[21] S. D. Murugan, D. Kumar, S. Bhattacharjee, and S. S. Ray, Many-body chaos in thermalized fluids, Phys. Rev. Lett. **127**, 124501 (2021).
[22] S. Mukherjee, R. K. Singh, M. James, and S. S. Ray, Intermittency, fluctuations and maximal chaos in an emergent universal state of active turbulence, Nat. Phys. **19**, 891 (2023).
[23] P. A. Davidson, *Turbulence in Rotating, Stratified and Electrically Conducting Fluids* (Cambridge University Press, Cambridge, 2013).
[24] J. J. Riley and M.-P. Lelong, Fluid motions in the presence of strong stable stratification, Annu. Rev. Fluid Mech. **32**, 613 (2000).
[25] C. Staquet and J. Sommeria, Internal gravity waves: From instabilities to turbulence, Annu. Rev. Fluid Mech. **34**, 559 (2002).
[26] C. P. Caulfield, Layering, instabilities, and mixing in turbulent stratified flows, Annu. Rev. Fluid Mech. **53**, 113 (2021).
[27] C.-C. P. Caulfield, Open questions in turbulent stratified mixing: Do we even know what we do not know? Phys. Rev. Fluids **5**, 110518 (2020).
[28] P. F. Linden, Mixing in stratified fluids, Geophys. Astrophys. Fluid Dyn. **13**, 3 (1979).
[29] J. J. Riley, R. W. Metcalfe, and M. A. Weissman, Direct numerical simulations of homogeneous turbulence in density-stratified fluids, AIP Conf. Proc. **76**, 79 (1981).
[30] H. J. S. Fernando, The growth of a turbulent patch in a stratified fluid, J. Fluid Mech. **190**, 55 (1988).
[31] E. C. Itsweire and K. N. Helland, Spectra and energy transfer in stably stratified turbulence, J. Fluid Mech. **207**, 419 (1989).
[32] B. R. Ruddick, T. J. McDougall, and J. S. Turner, The formation of layers in a uniformly stirred density gradient, Deep Sea Res. A. Oceanogr. Res. Papers **36**, 597 (1989).
[33] Y.-G. Park, J. A. Whitehead, and A. Gnanadeskian, Turbulent mixing in stratified fluids: Layer formation and energetics, J. Fluid Mech. **279**, 279 (1994).
[34] F. Nicolleau and J. C. Vassilicos, Turbulent diffusion in stably stratified non-decaying turbulence, J. Fluid Mech. **410**, 123 (2000).
[35] P. Billant and J.-M. Chomaz, Self-similarity of strongly stratified inviscid flows, Phys. Fluids **13**, 1645 (2001).

[36] J.-P. Laval, J. C. McWilliams, and B. Dubrulle, Forced stratified turbulence: Successive transitions with Reynolds number, Phys. Rev. E **68**, 036308 (2003).
[37] E. Lindborg, The energy cascade in a strongly stratified fluid, J. Fluid Mech. **550**, 207 (2006).
[38] E. Lindborg and G. Brethouwer, Vertical dispersion by stratified turbulence, J. Fluid Mech. **614**, 303 (2008).
[39] P. Augier, S. Galtier, and P. Billant, Kolmogorov laws for stratified turbulence, J. Fluid Mech. **709**, 659 (2012).
[40] Y. Kimura and J. R. Herring, Energy spectra of stably stratified turbulence, J. Fluid Mech. **698**, 19 (2012).
[41] C. Rorai, P. D. Mininni, and A. Pouquet, Stably stratified turbulence in the presence of large-scale forcing, Phys. Rev. E **92**, 013003 (2015).
[42] C. Herbert, R. Marino, D. Rosenberg, and A. Pouquet, Waves and vortices in the inverse cascade regime of stratified turbulence with or without rotation, J. Fluid Mech. **806**, 165 (2016).
[43] A. V. Glazunov, E. V. Mortikov, K. V. Barskov, E. V. Kadantsev, and S. S. Zilitinkevich, Layered structure of stably stratified turbulent shear flows, Izv. Atmos. Oceanic Phys. **55**, 312 (2019).
[44] A. Maffioli, A. Delache, and F. S. Godeferd, Signature and energetics of internal gravity waves in stratified turbulence, Phys. Rev. Fluids **5**, 114802 (2020).
[45] V. Labarre, P. Augier, G. Krstulovic, and S. Nazarenko, Internal gravity waves in stratified flows with and without vortical modes, Phys. Rev. Fluids **9**, 024604 (2024).
[46] A. K. Varanasi, Lagrangian intermittency and vertical confinement in stably stratified turbulence, arXiv:2503.22445.
[47] M. F. Diaz and M. L. Waite, Predictability of decaying stratified turbulence, Phys. Fluids **36**, 065138 (2024).
[48] Y. Peng, X. Xu, Q. Shao, H. Weng, H. Niu, Z. Li, C. Zhang, P. Li, X. Zhong, and J. Yang, Applications of finite-time Lyapunov exponent in detecting Lagrangian coherent structures for coastal ocean processes: A review, Front. Mar. Sci. **11**, 1345260 (2024).
[49] S. Hariri, Analysis of mixing structures in the Adriatic Sea using finite-size Lyapunov exponents, Geophys. Astrophys. Fluid Dyn. **116**, 20 (2022).
[50] J. H. Bettencourt, C. López, and E. Hernández-García, Characterization of coherent structures in three-dimensional turbulent flows using the finite-size Lyapunov exponent, J. Phys. A: Math. Theor. **46**, 254022 (2013).
[51] G. K. Vallis, *Atmospheric and Oceanic Fluid Dynamics: Fundamentals and Large-Scale Circulation*, 2nd ed. (Cambridge University Press, Cambridge, 2017).
[52] M. L. Waite and P. Bartello, Stratified turbulence dominated by vortical motion, J. Fluid Mech. **517**, 281 (2004).
[53] A. Maffioli, G. Brethouwer, and E. Lindborg, Mixing efficiency in stratified turbulence, J. Fluid Mech. **794**, R3 (2016).
[54] G. Brethouwer, P. Billant, E. Lindborg, and J.-M. Chomaz, Scaling analysis and simulation of strongly stratified turbulent flows, J. Fluid Mech. **585**, 343 (2007).
[55] W. J. Emery, W. G. Lee, and L. Magaard, Geographic and seasonal distributions of Brunt–Väisälä frequency and Rossby Radii in the North Pacific and North Atlantic, J. Phys. Oceanogr. **14**, 294 (1984).
[56] R. C. Millard, W. B. Owens, and N. P. Fofonoff, On the calculation of the Brunt-Väisäla frequency, Deep Sea Res. A. Oceanogr. Res. Papers **37**, 167 (1990).
[57] K. Shahzadi and N. Pinardi, SeaDataCloud Brunt–Väisälä Frequency profiles for the Atlantic and Pacific Oceans, Ref. Product Information Document (PIDoc), SeaDataCloud 2021, https://doi.org/10.13155/79296.
[58] E. M. Stanley and R. C. Batten, Viscosity of sea water at moderate temperatures and pressures, J. Geophys. Res. **74**, 3415 (1969).
[59] R.-C. Lien and M. C. Gregg, Observations of turbulence in a tidal beam and across a coastal ridge, J. Geophys. Res.: Oceans **106**, 4575 (2001).
[60] J. Jiménez, Oceanic turbulence at millimeter scales, Oceanogr. Lit. Rev **3**, 598 (1998).

[61] S. D. Murugan and S. S. Ray, Genesis of thermalization in the three-dimensional, incompressible, Galerkin-truncated Euler equation, Phys. Rev. Fluids **8**, 084605 (2023).
[62] H. Hanazaki and J. C. R. Hunt, Linear processes in unsteady stably stratified turbulence, J. Fluid Mech. **318**, 303 (1996).
[63] R. D. J. G. Ho, A. Berera, and D. Clark, Chaotic behavior of Eulerian magnetohydrodynamic turbulence, Phys. Plasmas **26**, 042303 (2019).